Corrosion Science 57 (2012) 114–121
DOI: http://dx.doi.org/10.1016/j.corsci.2011.12.027

On the oxidation mechanism of pure tungsten in the temperature range 600–800 °C

S.C. Cifuentes [a], M.A. Monge [b], P. Pérez [a,*]

[a] Departamento de Metalurgia Física, Centro Nacional de Investigaciones Metalúrgicas, CENIM-CSIC, Avda Gregorio del amo 8, 28040 Madrid, Spain
[b] Departamento de Física, Universidad Carlos III de Madrid, Avd de la Universidad 30, 28911, Spain

Abstract: The oxidation behavior of International Thermonuclear Experimental Reactor (ITER) reference tungsten grade has been evaluated in dry air in the temperature range 600 800 °C. At 600 °C, the scale remained protective while the integrity of $W_{18}O_{49}$ layer was kept. Rapid increase in mass gain resulted from mas sive cracking at local areas in the $W_{18}O_{49}$ layer. Then, a coarse non protective columnar $WO_{2.92}$ scale was developed which favoured rapid inward oxygen transport into the alloy. At 700 and 800 °C, growth stres ses in the scale were released through local cracking. At this stage, $WO_{2.92}$ became progressively trans formed into WO_3 when the oxygen partial pressure increased across the scale thickness.

Keywods: C. High temperature corrosion, C. Oxidation, C. Kinetic parameters.

1. Introduction

Selection of the plasma facing materials (PFMs), i.e. the materi als that will interact with the fusion plasma directly, is a critical is sue for the success of the ITER and the development of future fusion power plants [1 4]. PFMs will operate under extreme condi tions of temperature, irradiation and thermal stresses because of their direct exposure to the fusion plasma. Furthermore, material choice plays a central role in the environmental safety of fusion power reactors in future commercial energy plants [5,6]. A suitable PFM should contain elements of reduced activation in such a way that production of radioactive by products and tritium inventories are minimized [7]. These considerations as well as working condi tions of plasma facing components (PFCs) reduce the availability of material candidates to those based on C, V, W, Ti and Be [8].

However, PFCs based on low Z materials have a short erosion lifetime due to their high sputtering yields under the plasma par ticles bombardment and radiation enhanced sublimation [9]. Fur thermore, neutron irradiation increases tritium retention on beryllium and carbon base materials, rising safety hazards and reducing environmental attractiveness of fusion power plants due to accidental release of tritium and/or production of hazardous nuclear by products [7]. In addition, low melting point and high toxicity of beryllium have dissuaded about the use of this alloy in fusion reactors.

Properties such as very high melting point and very low vapor pressure, low sputtering yield, good thermal conductivity, low thermal expansion coefficient, high strength at high temperatures, low retention of tritium and good dimensional stability under neutron irradiation make tungsten, at present, the most promising candidate material for building divertor in PFCs at the ITER and fu ture fusion reactors. Its major drawback, however, is the poor oxi dation resistance which would cause irreversible detrimental effects on physical and chemical characteristics of W based com ponents [3,10]. Even though the PFCs will operate in vacuum con dition, fortuitous scenarios such as a LOCA event (Lost of Coolant Accident) or air ingress as a result of failure of the vessel's integrity, can lead to oxidizing atmospheres which will have harmful impact on the operation of PFCs [11,12]. In case of emergency shutdown of a fusion power reactor, the temperature of tungsten PFCs would re main above 450 °C for several weeks [12]. An oxidizing atmosphere at these temperatures would enhance the oxidation rate through the formation of highly volatile radioactive tungsten oxides [13]. Thus, an assessment of the oxidation characteristics of ITER grade W appears to be necessary to update the database of tungsten for fusion applications [8].

Oxidation of tungsten produced by different routes and with different grade of purity has been widely studied in the past [14 22]. These studies have concluded that the oxidation kinetics of tungsten is quite complex. This complexity arises from the wide variety of oxides formed during oxidation as well as the develop ment of stresses in the course of the oxidation. These two reasons seem to be the origin of the discrepancies regarding tungsten oxi dation, as clearly manifested in the excellent review by Ivanov et al. [23].

In this work, the oxidation behavior of ITER reference tungsten grade has been studied in dry air in the temperature range 600 800 °C. This study tries to: (i) Get better understanding on the oxidation mechanism of tungsten through the analysis of the structure and nature of the oxides composing the scale. (ii) Provide useful oxidation data on ITER reference tungsten grade.

* Corresponding author. Tel.: +34 915538900; fax: +34 915347425.
E-mail address: zubiaur@cenim.csic.es (P. Pérez).

2. Experimental procedure

Oxidation tests at 600 and 700 °C were carried out on disks, 10 mm in diameter and 1 mm thick, cut from a rod of a swaged ITER reference tungsten grade (99.97% purity). Tests at 800 °C were done on coupons $5 \times 5 \times 2$ mm^3. All major surfaces were abraded on successively finer silicon carbide papers, then mechanically pol ished with 1 μm diamond paste and cleaned with ethanol. Oxidation kinetics were determined by continuous isothermal thermogravi metry tests in the temperature range 600 800 °C for exposures up to 100 h. At 800 °C, exposure time was reduced to 20 h because the high mass gain of samples implied the risk of exceeding the maximum weight range of the microbalance. Oxidation tests were carried out under dry synthetic air (dewpoint below −40 °C).

The characterization of oxidation products was performed on samples used for mass gain determination, as well as on samples isothermally oxidized for different exposure times. Cross sections were prepared by conventional metallographical techniques. To prevent scale loss during the metallographic preparation of the sample, the surfaces were coated first with a thin gold layer (by sputtering) and then with a thicker layer of copper (electrolytically deposited). Surfaces and cross sections of the oxidized specimens were studied by scanning electron microscopy (SEM). Phase iden tification of the oxide scale was performed by X ray diffraction (XRD) using Co K_α radiation and energy dispersive X ray micro analysis (EDX).

3. Results

3.1. Microstructure

Fig. 1 shows transverse and longitudinal views of the tungsten rod. The columnar structure was revealed by etching the surfaces with Murakami's reagent (modified A). The microstructure con sisted of anisotropic elongated grains oriented along the axis of the rod (see inset on Fig. 1). The grain orientation in coupons was perpendicular to the major surfaces, which corresponds to current ITER specifications for the use of tungsten as material in PFCs [8,24].

3.2. Oxidation kinetics

The mass gain curves in dry air at 600, 700 and 800 °C of tung sten processed by conventional techniques are shown in Fig. 2. Mass gain curves clearly proved that the oxidation resistance of pure tungsten decreases substantially above 600 °C. The kinetics were determined by adjusting the mass gain curves to a power law of the form $\Delta W = kt^n$ (ΔW is the mass gain per unit area, k the oxidation rate constant, n the rate exponent, and t the exposure time). Changes in the kinetic laws governing the oxidation behav ior could be noticed in the course of the exposure at a given tem perature, as presented in Table 1. The oxidation kinetics at 600 °C were governed by almost parabolic laws, $n \approx 0.7$, beyond the ini tial transient state. At 700 °C a significant increment in the mass gain was measured, about one order of magnitude higher than the measured at 600 °C (135 against 11.3 mg cm^{-2} respectively). During the initial stages of oxidation at 700 °C the material still fol lowed the almost parabolic behavior found at 600 °C. However, a progressive deviation of the initial almost parabolic behavior to wards a nearly linear law was observed after the first 2 h of expo sure. The kinetics at 800 °C obeyed linear laws from the initial stages of oxidation. It is interesting to note the mass gain after 20 h of exposure was comparable to that of the sample tested at 700 °C for 100 h.

3.3. X ray diffraction

Three oxides with monoclinic crystalline structure (WO_3, $W_{18}O_{49}$ and $WO_{2.92}$) were identified after exposure at 600 °C, as shown in XRD pattern of Fig. 3a. The most intense phase corre sponded to WO_3. The peaks assigned to $WO_{2.92}$ had an intermedi ate intensity, suggesting that this oxide was probably located in the innermost part of the oxide scale. It is worth noting that the oxide on the surface showed a yellowish color at this temperature, which coincides with WO_3 color.

Major difference of XRD patterns at 700 °C arose from the ab sence of $W_{18}O_{49}$ and $WO_{2.92}$ peaks (Fig. 3b). Absence of both oxides could be attributed to the limited penetration of X ray in a dense material with a high atomic number such as tungsten oxides, as well as the large thickness of the outer WO_3 layer. No formation or disappearance of these oxides in the course of oxidation at 700 °C could be another explanation. XRD patterns at 800 °C were not taken because the irregular growth of the oxide layer (much thicker in the edges than in the center of large smooth surfaces) precluded accurate XRD measurements. Since the structure of the scale at 800 °C for 20 h was similar to that developed after 100 h exposure at 700 °C (see electron microscope observations in the next section), no differences in the nature of the oxides formed

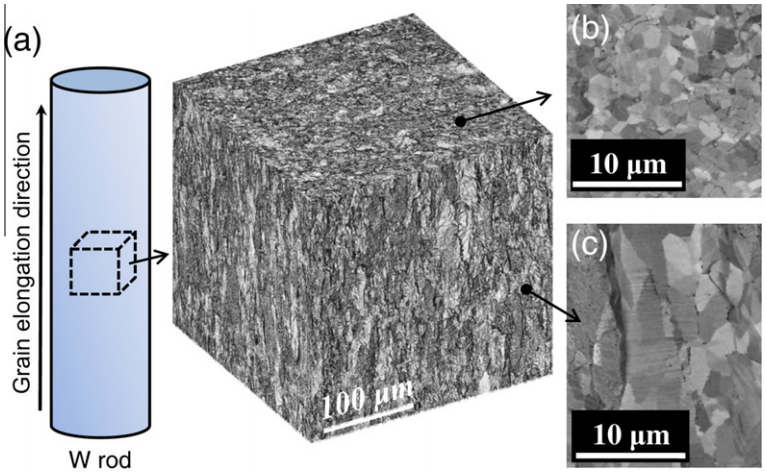

Fig. 1. (a) Composition of optical microscopy images showing the microstructure of the tungsten bar. (b) Backscattered image showing close magnification of the transverse section. (c) Backscattered image showing close magnification of the longitudinal section.

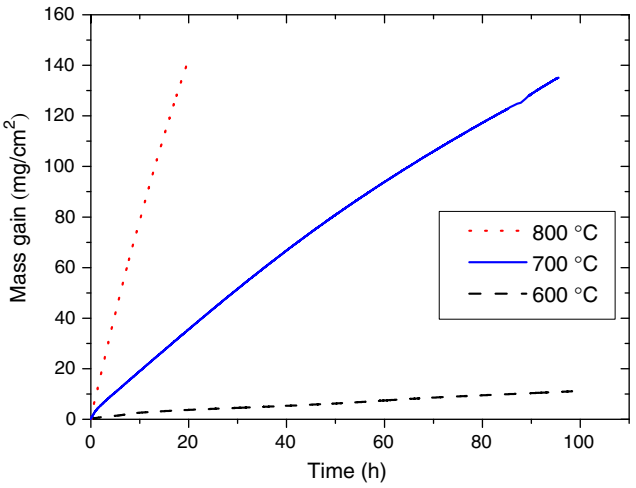

Fig. 2. Mass gain curves of pure tungsten in dry air between 600 and 800 °C.

Table 1
Values taken by the oxidation exponent during oxidation in air in the 600–800 temperature range.

Temperature (°C)	Time range (h)	*n*	Kinetics
600	0–100	0.7	Almost linear
700	0–2	0.7	Almost linear
	2–100	0.9	Almost linear
800	0–20	1	Linear

at both temperatures were expected. This agrees with XRD mea surements in the literature which found the same oxides during oxidation at 700 and 800 °C [15].

3.4. Oxidized surfaces

Fig. 4 shows the surface of the scale after oxidation tests. At all temperatures, the external oxide scale was constituted by equi axed crystals whose size increased with increasing the oxidation temperature. Thus, crystal size ranged between 100 and 200 nm after 100 h at 600 °C and 300 600 nm after exposure for 20 h at 800 ° C. During cooling from 700 °C to room temperature, cracking of the scale took place and the scale partially spalled off during subsequent handling. Detachment proceeded along preferential planes parallel to the surface, conferring a stratified appearance to the surface. Significant differences were noticed among de tached and non detached regions. At low magnifications numerous interconnected cracks could be observed over the entire surface of detached regions (innermost part of the scale), as shown in Fig. 5a. On the other hand, some large cracks and incipient non intercon nected secondary cracking were found in non detached regions, as shown in Fig. 5b. Cracking could be either related to the large volume change associated with oxide formation or could be in duced by thermal stresses generated during cooling. Analyses on the surface of detached and non detached regions also evidenced changes in the structure and morphology of the scale. Thus, the outer scale was relatively dense, excluding the regions with cracks, and constituted by equiaxed grains with sizes ranging between 150 and 400 nm after 100 h of exposure (see Fig. 4b). On the other

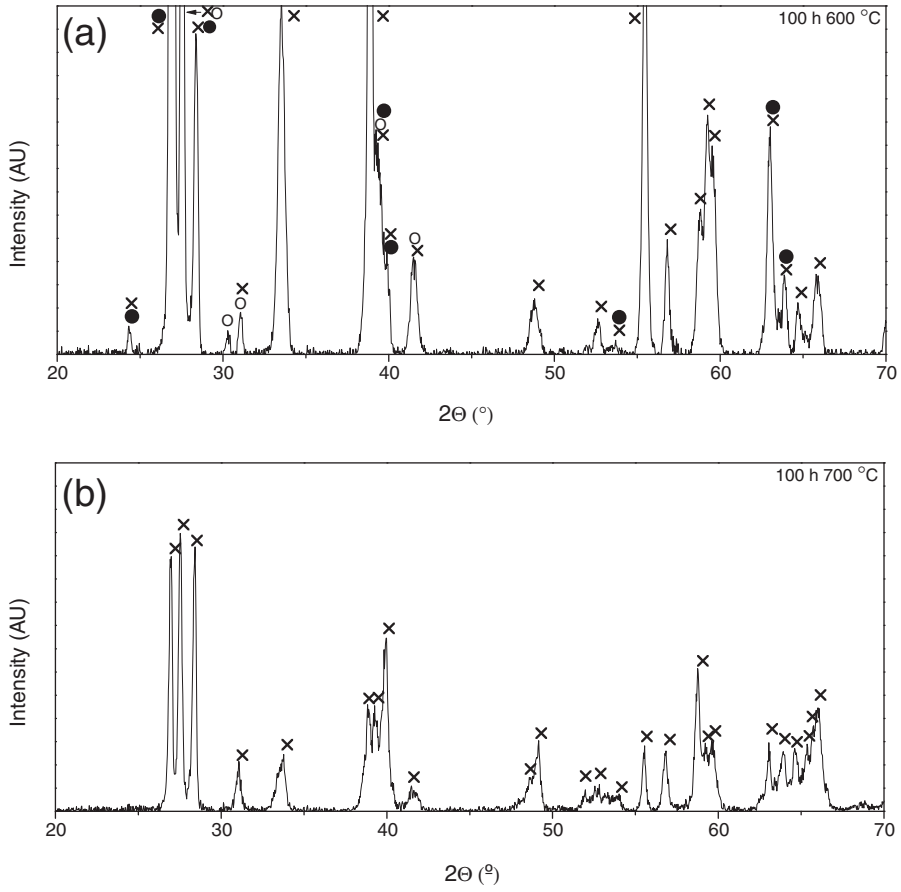

Fig. 3. XRD patterns (normal incidence) of tungsten samples oxidized in dry air for 100 h: (a) enlargement of low intensity part of XRD pattern at 600 °C. (b) 700 °C. ×, WO_3, ○, $W_{18}O_{49}$, ●, $WO_{2.92}$.

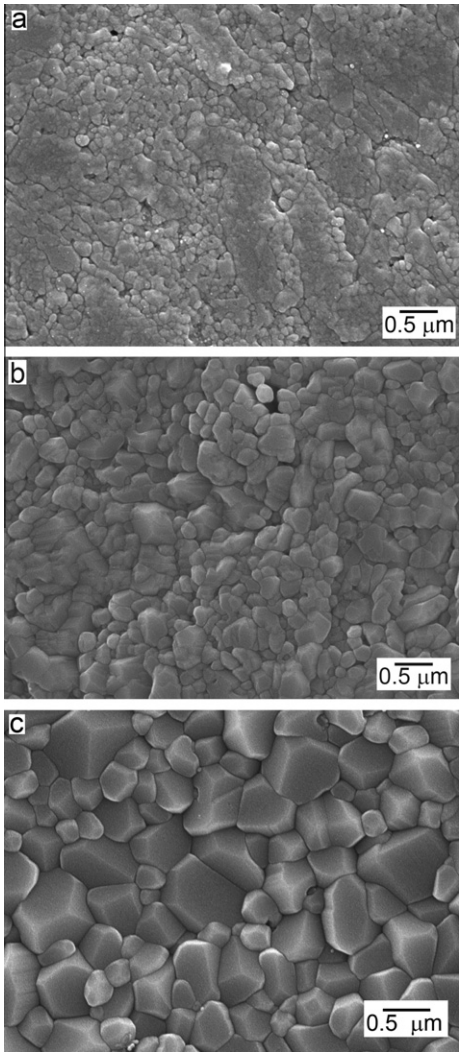

Fig. 4. Surface of the samples oxidized in air: (a) 100 h 600 °C. (b) 100 h 700 °C. (c) 20 h 800 °C.

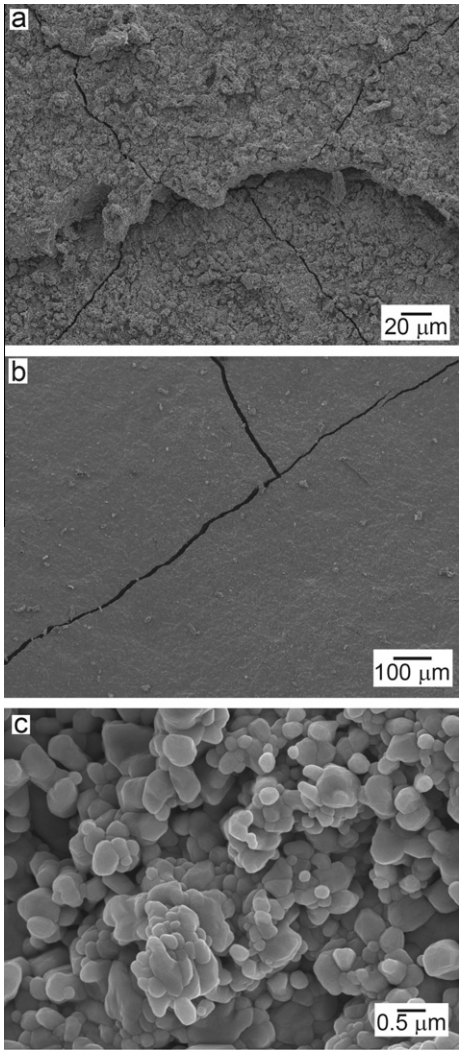

Fig. 5. Surface of the samples oxidized in air after 100 h exposure at 700 °C: (a) detached region, (b) non-detached region, (c) detail of oxide structure in detached regions.

hand, spalling permitted to distinguish the porous nature of the in ner oxide scale, as shown in Fig. 5c. Crystal size of this inner oxide was coarser, between 200 nm and 1 μm, than that corresponding to the outermost oxide.

Similar features were found after exposure at 800 °C for 20 h, although no spalling took place during cooling. As seen in the sam ple oxidized at 700 °C, big cracks and non interconnected second ary cracks were also present on the surface. Observation of the oxide scale on the edges proved the non equiaxed nature of oxide crystal, as shown in Fig. 6. The columnar morphology of the oxides can be clearly checked, with lengths up to 2 3 μm, leaving numer ous cavities during their growth. Therefore, the equiaxed appear ance on the external surface arose from the normal view of oxide crystals with respect to the growth direction.

3.5. Cross sectional views

Fig. 7 shows a relatively dense oxide scale of about 50 μm formed after exposure for 50 h at 600 °C. The oxide scale seems to be composed of two layers; a thin outermost layer of about 8 μm and a thicker innermost layer of about 40 μm. The existence of a nearly continuous band of cavities between both layers clearly depicts both parts of the scale. Some cavities also extend from the boundary between both layers towards the gas surface. Moreover, some of the isolated pores in the outermost layer are aligned along the same direction, as marked by the line in Fig. 7. Just beneath the boundary, in a region of about 10 μm, the innermost layer contains abundant voids and porosity. Some of them coalesce to produce large cavities although they are not connected. Underlying this re gion the layer becomes denser, with very little porosity. Neverthe less, voids and large cavities are again concentrated during further growth. The structure of the oxide layer formed after 100 h of exposure is identical to that observed for 50 h, as shown in Fig. 8. The thickness of the oxide scale is about 95 μm. The scale may be divided into the same two layers. The structure and thick ness of the outermost layer (about 10 μm) are practically identical to that found after 50 h of exposure. This clearly indicates that the oxide scale grows by inward oxygen diffusion. On the other hand, the innermost layer thickens steadily in the course of the oxida tion. Once more this layer consists of alternating regions with low and high pores, voids or cavities. Either cracks running throughout the oxide scale from the oxide/metal interface to the gas/oxide interface or cracks running parallel to the oxide/metal interface are observed.

Figs. 9 and 10 show the oxide layer formed at 700 and 800 °C, respectively. Both layers have a stratified structure. At 700 °C, a porous structure 800 μm thick formed beneath the compact outer

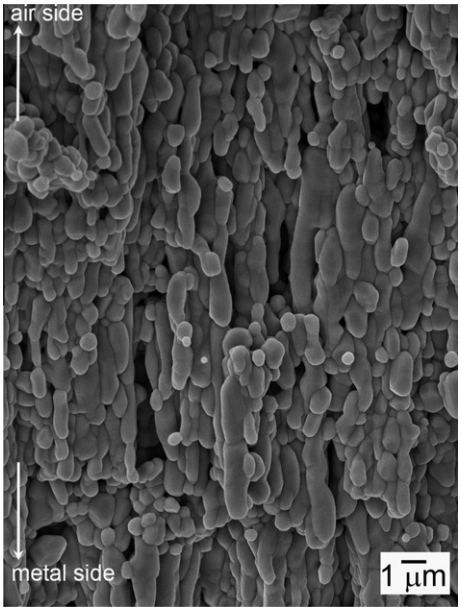

Fig. 6. Cross sectional view of the scale developed on the edges of the sample oxidized in air after 20 h exposure at 800 °C.

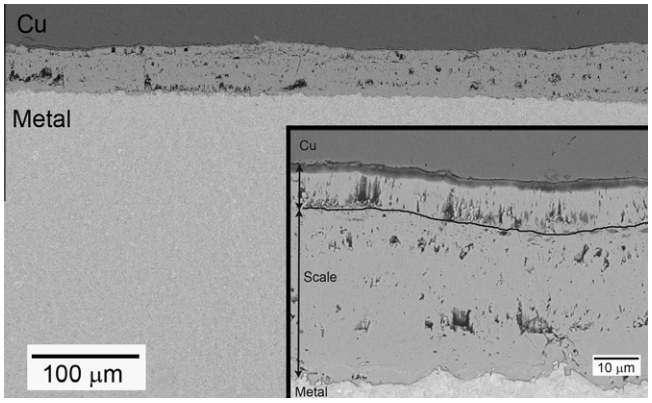

Fig. 7. Cross section of the scale developed on the sample oxidized in air after 50 h exposure at 600 °C. The inset shows a detail of the oxide scale.

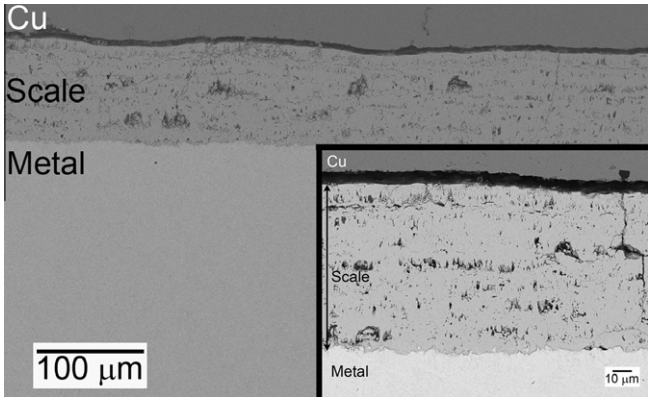

Fig. 8. Cross section o the scale developed on the sample oxidized in air after 100 h exposure at 600 °C. The inset shows a close magnification of the scale.

layer of not more than 10 μm in thickness. At 800 °C, the scale thickness reaches 1.15 mm. Each layer within the stratified structure is separated from each other by interconnected cavities. Although the test at 800 °C was only carried out during 20 h, the thickness of the oxide scale is 1.5 times larger than that of the scale formed at 700 °C after 100 h of oxidation.

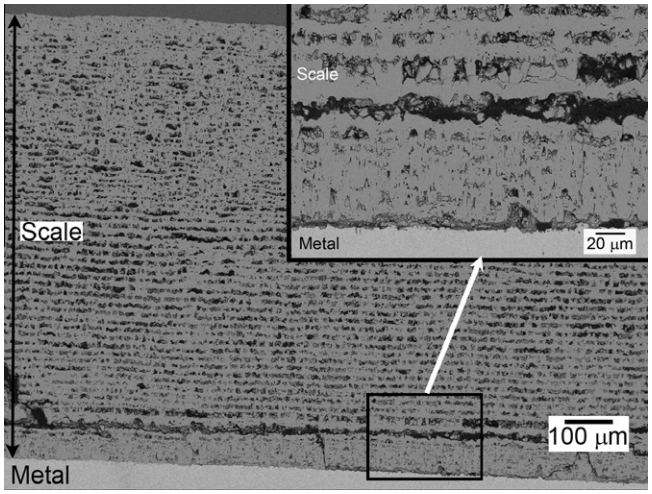

Fig. 9. Cross section o the scale developed on the sample oxidized in air after 100 h exposure at 700 °C. The inset shows the scale close to the oxide/metal interface marked.

4. Discussion

The results evidence the complexity of tungsten oxidation. This agrees with the numerous discrepancies reported in the literature concerning kinetics, composition and structure of the oxide scale [14 23]. Although the change from parabolic to linear kinetics has been described during oxidation in the temperature range 500 700 ° C [14,18], a parabolic behavior was not found in our study over the entire temperature range. Furthermore, our results differ from the data reported in previous works in which kinetics obeyed parabolic laws during short term exposure in the interval 400 900 °C [14,20,25]. This means that the oxide scale was unable to provide effective protection from the early stages of oxidation, as deduced by the lateness for achieving the steady state. More over, mass gain rate was increased after exposure for 6 h, as marked in the mass gain curve of Fig. 11. This suggests that the slight protective nature of the initial scale was lost after this peri od. Additional time was required for recovering the healing nature of the oxide scale until new impairment of the scale took place (at about 50 h). Then, a new steady state would be attained until a new event of protectiveness loss would take place.

XRD data proved that the scale at 600 °C consisted of different oxides with the following sequence, from the outer surface to wards the inner metal, WO_3, $W_{18}O_{49}$ and $WO_{2.92}$. The yellow color of external oxide confirmed that WO_3 was mostly located in the outer part of the scale. This coincides with some studies reported in the literature [14,15,18 21,26]. Nevertheless, other authors have described the formation of a protective dark layer [15,20,21,26]. Discrepancies could result from the different expo sure times used in these works. Moreover, the influence of impuri ties cannot be ruled out because the reduction kinetics of non sag (NS) doped tungsten blue oxide is affected strongly by small amounts of impurities such K, Al or Si [27]. Usually, the typical yel low color of WO_3 was not observed during short term exposures, up to 6 h, between 500 and 700 °C [14], which would confirm that WO_3 formed once a continuous dark layer was established. Kellet et al. attributed it to $W_{18}O_{49}$ oxide [15]. Furthermore, Webb et al. found a dark blue layer, presumably W_4O_{11}, after scraping the

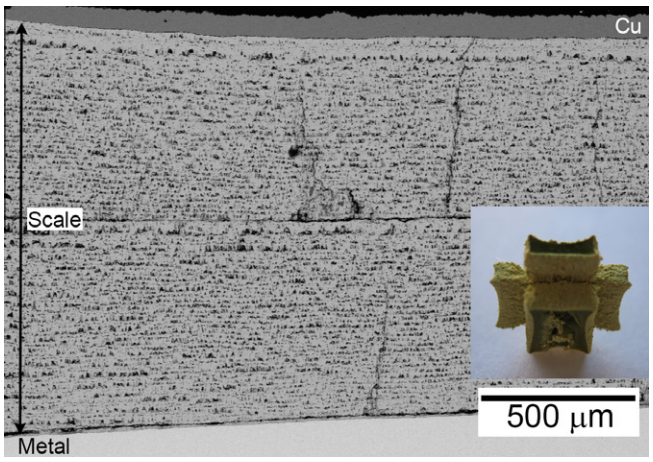

Fig. 10. Cross section o the scale developed on the sample oxidized in air after 20 h exposure at 800 °C. The inset shows the sample after oxidation test.

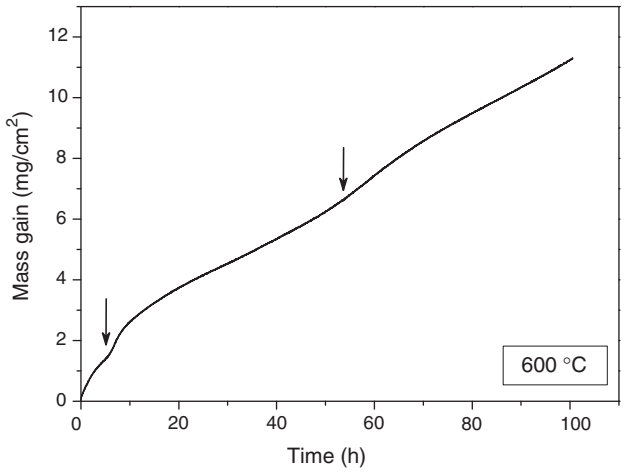

Fig. 11. Mass gain curve of the sample oxidized 100 h at 600 °C in dry air. Arrows indicate points at which protective nature of the scale was lost.

external yellow scale in a sample oxidized 4 h at 700 °C [20]. Other authors concluded that this layer corresponded to WO_2 [26]. T o check this point, a sample was oxidized for 1 h. Visual aspect of the sample evidences a black thin layer. XRD pattern of Fig. 12, ta ken with an incidence of 5°, proved that maximum intensity peak corresponded to $W_{18}O_{49}$. Intense $WO_{2.92}$ peaks were already pres ent (right and left shoulders of the most intense peaks) after this short exposure time.

Cross sectional views revealed a relatively dense scale, but curi ously, a nearly continuous band of cavities, many times intercon nected, was present underlying the outermost external layer. Formation of these cavities was, obviously, related to the first point in the mass gain curve at 600 °C where an increase in the oxidation rate was observed. Microcracking in the WO_3 layer has been sug gested to promote the change from parabolic to linear laws be cause of the formation of transversal cracks throughout the scale [14]. Cracking of the oxide scale could be expected because of the significant volume change resulting from the oxidation of tung sten into any kind of tungsten oxide (Pilling Bedworth ratio of 3.3 for WO_3). The high compression stresses arising from oxide growth were stored in the scale and mostly released during cracking events. Although some transversal cracks could be also found crossing thoroughly the oxide scale, the absence of localized attack in the metal, ahead the crack tip, implies that accelerated oxide growth cannot be associated with transversal cracking. Probably, these transversal cracks could be originated by the stresses gener ated during cooling as a result of: (i) large differences among ther mal expansion coefficients of tungsten and tungsten oxides and/or (ii) volume changes induced by allotropic transformation of tung sten oxides. At the temperatures used in this work, the orthorhom bic structure transformed into monoclinic WO_3 during cooling. The volume change (ΔV) can be calculated as $\Delta V = (V_{mon} - V_{ort})/V_{ort}$. Ta ken V_{ort} = 430.90 and V_{mon} = 146.69 from XRD standard patterns of monoclinic (pattern 00 054 0508) and orthorhombic WO_3 (pattern 01 071 0131), ΔV = 0.66 (shrinkage of 66%).

The oxidation was divided into different stages, illustrated in the scheme of Fig. 13. Basically, growth stresses induced during oxidation were released by cracking of the scale. This cracking was limited to a small restricted region. In these regions two pro cesses or phenomena occurred simultaneously. In the neighbor non cracked region, oxidation proceeded normally. New oxide for mation was accompanied by a considerable volume increase which could be accommodated by moving the scale outwards. Although oxygen transport across the crack occurred quickly, some time was required before oxygen could be transported from the top side to the bottom side of the crack. In the meantime, the scale shifted continuously outwards, leading to crack enlargement in such a way that cracks tended progressively to appear as voids or cavities. The enlargement of voids was halted when new oxide formed at the bottom side of cavities. At this point, oxide continued to form as a continuous layer until growth stresses were again released through local cracking events. This mechanism explains the multi layered appearance of the scale in which a porous band was fol lowed by a relatively dense layer.

Impairment or cracking of the oxidation scale led to the change in the structure of the oxide underlying this region. The structure become columnar, with grains orientated perpendicularly to the scale/substrate interface. This configuration facilitated rapid

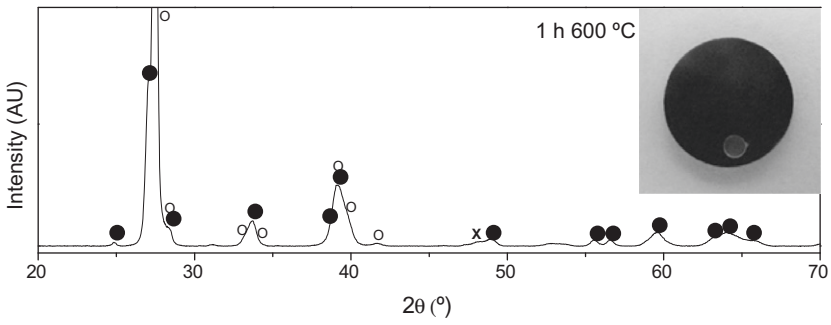

Fig. 12. XRD pattern (incidence angle of 5°) of tungsten sample oxidized at 600 °C for 1 h in dry air. ○, $W_{18}O_{49}$, ●, $WO_{2.92}$, ×, W. The inset shows the black film formed on the sample after the oxidation test.

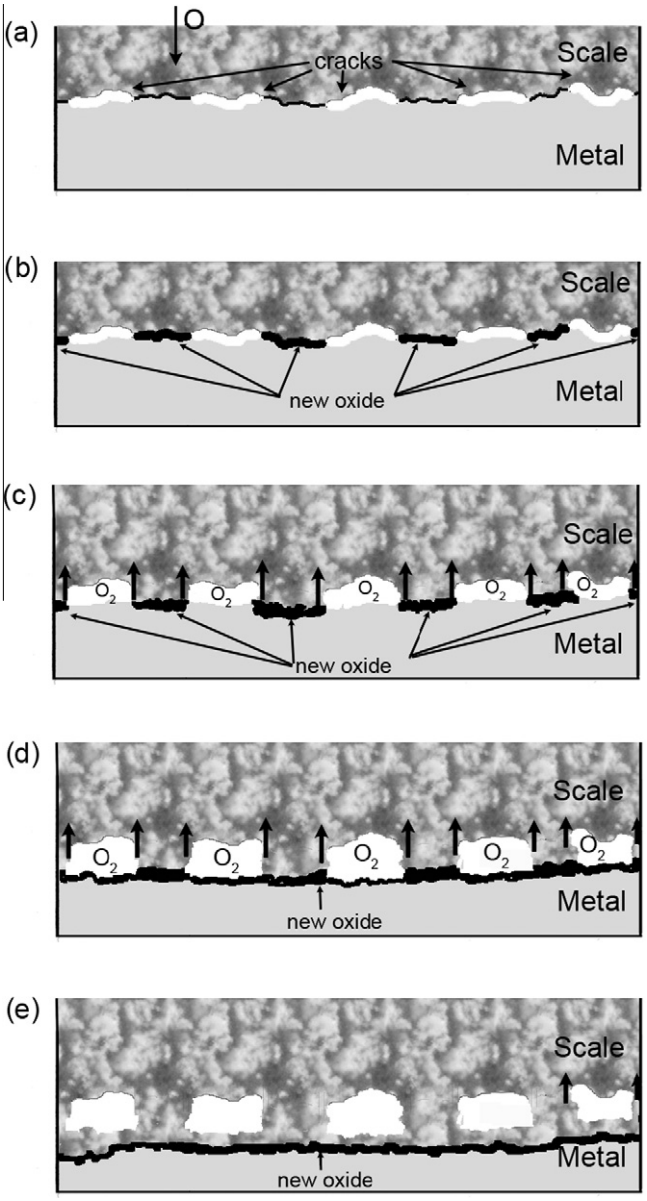

Fig. 13. Scheme illustrating the different stages of cavity formation: (a) Local cracking of the oxide scale at the scale/metal interface. (b) New oxide formed on non-cracked areas grows outward. The crack grows. (c) Cavities are filled by oxygen gas. (d) New oxide is generated over the entire scale/metal interface when pressure is enough high to proceed with oxidation at the bottom of the cavity. (e) Cavities remain embedded in the scale.

oxygen ingress towards the metal substrate and could explain why the kinetics became higher than parabolic ($n \approx 0.7$). Moreover, the columnar structure accounted for the outward growth of the scale in spite oxide growth took place by oxygen transport towards the scale/metal interface [14,25]. According to the XRD pattern of the sample exposed for 40 h (only one cracking event in mass gain curve), this phase should correspond to $WO_{2.92}$. Outward growth mode was maximized when $WO_{2.92}$ is formed instead of WO_3 because volume change is much higher for $WO_{2.92}$ formation than for WO_3 formation.

The oxidation mechanism was exacerbated at 700 and 800 °C. Thus, almost linear kinetics became linear after 2 h of exposure at 700 °C whereas kinetics obeyed linear laws over the entire exposure at 800 °C. Cross sectional views clearly showed very thick porous scale whose morphology resembled quite well that of the multilayered scale developed during oxidation of pure titanium above 800 ° C [28,29]. Unlike the rutile scale formed on pure titanium, the continuous disruption or crack between individual layers was absent. Large cavities, sometimes connected, appeared instead. This agreed rather well with the mechanism proposed by Gulbransen and Andrews [14]. According to these authors, oxi dation proceeded through a cyclic mechanism involving periodical cracking at local areas when a dense oxide layer attained a critical thickness. The size of cavities was larger as temperature was in creased, indicating that new oxide growth at metal/oxide interface took place faster than pressure increase inside the crack to form new oxide at the bottom of the crack. The result is the enlargement of cavities embedded in the scale.

XRD patterns at 700 °C did not confirm the presence of $WO_{2.92}$. Such absence could be attributed to: (a) $WO_{2.92}$ was located inter nally, far from the surface and consequently out of the detection range of X ray or (b) $WO_{2.92}$ was transformed progressively into WO_3 in the course of the oxidation. To check this point the scale formed at 700 °C was detached from the surface and, then, pulver ized. The only phase detected in the powder was WO_3. This proved that $WO_{2.92}$ transformed into WO_3 when oxidation obeys linear kinetics. It is interesting to note that the oxide scale grows strongly outwards at 800 °C, as presented in the inset of Fig. 10. Although the total mass gain was very similar to the sample oxidized at 700 °C, the thickness of the scale was significantly larger, about 330 μm. The latter indicated the lower compactness of the scale developed at 800 °C. This agreed with microstructural features ob served in the scale as the maximum size of cavities was around 13 and 19 μm at 700 and 800 °C, respectively.

As was commented in the preceding discussion, the outer scale was always constituted by WO_3. The dark blue oxide formed after short exposure times indicated that $W_{18}O_{49}$ was formed from the initial stages of oxidation whereas WO_3 grew later. WO_3 required outward tungsten transport from the metal to the outer surface. Since rapid oxygen entrance to the metal/scale interface consumed all tungsten, outward tungsten diffusion should be negligible. In addition, high volume of tungsten atoms and low oxidation tem peratures should make it unexpected. Therefore, other mechanism should account for outward tungsten transport. Transport as vola tile tungsten oxide, probably, might be the most reasonable alter native. The stability of tungsten oxides is highly dependant on oxygen pressure, leading to the formation of oxides with different stoichiometries. Removal of oxygen from WO_3 results in lower oxi des (WO_{3-x}, $0 < x < 1$). The lower the oxygen partial pressure the lower the stoichiometry. At 700 and 800 °C, the pressure depen dence is as follows; WO_3, W O $_{2.92}$, W $_{18}O_{49}$ and WO_2 [30]. Initial for mation of $W_{18}O_{49}$ should fix the oxygen gradient entering into the metal substrate. Therefore, $WO_{2.92}$ formation should be unex pected unless the oxygen partial pressure would rise up to the level in which $WO_{2.92}$ could grow. These conditions would be achieved when cracking of $W_{18}O_{49}$ layer occurred and the oxygen pressure in cavities was increased. Then, oxygen pressure could rise up to the point that $WO_{2.92}$ could volatilize before transformation into WO_3 would take place. This WO_3 should be transported outwards, towards the outer surface. There, the increase in the oxygen pres sure should promote deposition.

5. Conclusions

From the present work the following conclusions can de drawn:

1. The oxidation was initially controlled by the development of a continuous $W_{18}O_{49}$ layer. Increase in the oxidation rate towards linear kinetics is due to local cracking of $W_{18}O_{49}$ layer.

2. At 600 °C, the scale provided some protection to pure tungsten because massive cracking was limited to very few events clearly viewed in mass gain curves. At 700 and 800 °C, oxidation pro ceeded through a cyclic mechanism involving periodical crack ing at local areas when a dense oxide layer attained a critical thickness.
3. Equiaxed structure of $W_{18}O_{49}$ layer changed to the columnar structure of the thick $WO_{2.92}$ formed after cracking of $W_{18}O_{49}$ layer. $WO_{2.92}$ was progressively transformed into WO_3 in the course of the oxidation.
4. $WO_{2.92}$ volatilization transported tungsten outwards, towards the gas surface, leading to the formation of the yellow external WO_3 layer.

Acknowledgments

This investigation was supported by the Spanish Ministry of Science and Innovation (ENE2008 06,403 C06 04). The financial support from the Comunidad de Madrid, through the program TECHNOFUSION, Grant S2009/ENE 1679, is also gratefully acknowledged.

References

[1] E.E. Bloom, J.T. Busby, C.E. Duty, P.J. Maziasz, T.E. McGreevy, B.E. Nelson, B.A. Pint, P.F. Tortorelli, S.J. Zinkle, Critical questions in materials science and engineering for successful development of fusion power, J. Nucl. Mater. 367–370 (2007) 1–10.
[2] V. Barabash, G. Federici, R. Matera, A.R. Raffray, I.T.E.R. Home Teams, Armour materials for the ITER plasma facing components, Phys. Scr. T81 (1999) 74–83.
[3] M. Rieth, J.L. Boutard, S.L. Dudarev, T. Ahlgren, S. Antusch, et al., Review on the EFDA programme on tungsten materials technology and science, J. Nucl. Mater., in press. doi:10.1016/j.jnucmat.2011.01.075.
[4] H. Bolt, V. Barabash, W. Krauss, J. Linke, R. Neu, S. Suzuki, N. Yoshida, Materials for the plasma-facing components of fusion reactors, J. Nucl. Mater. 329–333 (2004) 66–73.
[5] D.A. Petti, K.A. McCarthy, W. Gulden, S.J. Piet, Y. Seki, B. Kolbasov, An overview of safety and environmental considerations in the selection of materials for fusion facilities, J. Nucl. Mater. 233–237 (part I) (1996) 37–43.
[6] H. Aytekin, E. Tel, R. Baldik, A. Aydin, An investigation for ground state features of some structural fusion materials, J. Fusion Energ. 30 (2011) 21–25.
[7] R.A. Causey, J.N. Brooks, G. Federici, Tritium inventory and recovery in next-step fusion devices, Fusion Eng. Des. 61–62 (2002) 525–536.
[8] Materials Assessment Report (MAR), ITER Doc. G 74 MA 10 01-07-11 W 0.2, 2001.
[9] R. Behrisch, G. Federici, A. Kukushkin, D Reiter, Material erosion at the vessel walls of future fusion, J. Nucl. Mater. 313–316 (2003) 388–392.
[10] V. Philipps, R. Neu, J. Rapp, U. Samm, M. Tokar, T. Tanabe, M. Rubel, Comparison of tokamak behavior with tungsten and low-Z plasma facing materials, Plasma Phys. Control. Fusion 42 (2000) B293–B310.
[11] J. Roth, E. Tsitrone, A. Loarte, Plasma-wall interaction: important ion induced surface processes and strategy of the EU task force, Nucl. Instrum. Meth. B 258 (2007) 253–263.
[12] V. Tang, R.R. Parker, Temperature transients of a fusion–fission ITER pebble bed reactor in loss of coolant accident, Fusion Eng. Des. 65 (2003) 11–26.
[13] Y.A. Yang, Y. Ma, J.N. Yao, B.H. Loo, Simulation of the sublimation process in the preparation of photochromic WO3 film by laser microprobe mass spectrometry, J. Non-Cryst. Solids 272 (2000) 71–74.
[14] E.A. Gulbransen, K.F. Andrew, Kinetics of the oxidation of pure tungsten from 500 to 1300 °C, J. Electrochem. Soc. 107 (1960) 619–628.
[15] E.A. Kellet, S.E. Rogers, The structure of oxide layers on tungsten, J. Electrochem. Soc. 110 (1963) 502–504.
[16] C.J. Rosa, G.C. Chen, V.K. Sikka, Oxidation mechanism of niobium (673–823 K) and tungsten (773–973 K), Z. Metallk. 71 (1980) 529–534.
[17] E.A. Gulbransen, K.F. Andrew, F.A. Brassart, Kinetics of oxidation of pure tungsten, 1150–1615 °C, J. Electrochem. Soc. 111 (1964) 103–109.
[18] E.A. Gulbransen, W.S. Wysong, Thin oxide films on tungsten, Trans. AIME 175 (1948) 611–627.
[19] E. Nachtigall, Eigenschaften von molybdän und wolfram bei niedrigen und mittleren temperaturen, Z. Metallk. 43 (1952) 23–26.
[20] W.W. Webb, J.T. Norton, C. Wagner, Oxidation of tungsten, J. Electrochem. Soc. 103 (1956) 107–111.
[21] J.P. Baur, D.W. Bridges, W.M. Fassell Jr., High pressure oxidation of metals—Tungsten in oxygen, J. Electrochem. Soc. 103 (1956) 266–272.
[22] W.B. Jepson, D.W. Aylmore, The formation of porous oxides on metals. II. Tungsten and the paralinear rate law, J. Electrochem. Soc. 108 (1961) 942–947.
[23] V.Y. Ivanov, Y.P. Nechiporenko, L.N. Yefimenko, M.I. Yurchenko, High temperature oxidation protection of tungsten, NASA Tecnichal Traslations, NASA TT F-583, 1969, Translation from "Atom" Press, 1968.
[24] T. Hirai, G. Pintsuk, J. Linke, M. Batilliot, Cracking failure study of ITER-reference tungsten grade under single pulse thermal shock loads at elevated temperatures, J. Nucl. Mater. 390–391 (2009) 751–754.
[25] V.K. Sikka, C.J. Rosa, The oxidation kinetics of tungsten and the determination of oxygen diffusion coefficient in tungsten trioxide, Corros. Sci. 20 (1980) 1201–1219.
[26] J.W. Hickman, E.A. Gulbransen, An electron diffraction study of oxide films formed on molybdenum tungsten, and alloys of molybdenum, tungsten and nickel, Trans. AIME 171 (1947) 371–388.
[27] W.D. Schubert, B. Lux, B. Zeiler, Formation and incorporation of dopant phases during technical reduction of NS-doped tungsten blue oxide, Int. J. Refract. Met. Hard Mater. 13 (1995) 119–135.
[28] P. Pérez, V.A.C. Haanappel, M.F. Stroosnijder, The effect of niobium on the oxidation behavior of titanium in N2/20% O2 atmospheres, Mater. Sci. Eng. A284 (2000) 126–137.
[29] P. Pérez, On the influence of water vapour on the oxidation behavior of pure Ti, Corros. Sci. 49 (2007) 1172–1185.
[30] J.P. Bonnet, J. Nowotny, M. Onillon, I. Sikora, Surface electrical properties of tungsten oxides in equilibrium with the gas phase, Oxid. Met. 13 (1979) 273–282.